J. Phys.: Condens. Matter **21** (2009) 474215 (9pp) doi:10.1088/0953-8984/21/47/474215

Broad-band dielectric spectroscopy and ferroelectric soft-mode response in the $Ba_{0.6}Sr_{0.4}TiO_3$ solid solution

T Ostapchuk[1], J Petzelt[1], J Hlinka[1], V Bovtun[1], P Kužel[1], I Ponomareva[2,4], S Lisenkov[2,4], L Bellaiche[2], A Tkach[3,5] and P Vilarinho[3]

[1] Institute of Physics, Na Slovance 2, 18221 Prague 8, Czech Republic
[2] Physics Department, University of Arkansas, Fayetteville, AR 72701, USA
[3] Department of Ceramics and Glass Engineering, CICECO, University of Aveiro, 3810-193 Aveiro, Portugal

E-mail: ostapcuk@fzu.cz

Received 14 April 2009, in final form 10 June 2009
Published 5 November 2009
Online at stacks.iop.org/JPhysCM/21/474215

Abstract

Ceramic $Ba_{0.6}Sr_{0.4}TiO_3$ (BST-0.6) samples were studied in the broad spectral range of 10^6–10^{14} Hz by using several dielectric techniques in between 20 and 800 K. The dominant dielectric dispersion mechanism in the paraelectric phase was shown to be of strongly anharmonic soft-phonon origin. The whole soft-mode response in the vicinity of the ferroelectric transition was shown to consist of two coupled overdamped THz excitations, which show classical features of a coupled soft and central mode, known from many ferroelectric crystals with a dynamics near the displacive and order–disorder crossover. Similar behaviour has been recently revealed and theoretically simulated in pure $BaTiO_3$ (see Ponomareva *et al* 2008 *Phys. Rev.* B **77** 012102 and Hlinka *et al* 2008 *Phys. Rev. Lett.* **101** 167402). Also for the BST system, this feature was confirmed by the theory based on molecular dynamics simulations with an effective first-principles Hamiltonian. In all the ferroelectric phases, additional relaxation dispersion appeared in the GHz range, assigned to ferroelectric domain-wall dynamics. The microwave losses were analysed from the point of view of applications. The paraelectric losses above 1 GHz are comparable with those in single crystals and appear to be of intrinsic multi-phonon origin. The ceramic BST system is therefore well suited for applications in the whole microwave range.

(Some figures in this article are in colour only in the electronic version)

1. Introduction

Barium strontium titanate $Ba_xSr_{1-x}TiO_3$ (BST-x) solid solution is a classical prototypic ferroelectric system (studied since 1946 [1]), with a simple perovskite structure. Its well defined ferroelectric phase-transition temperature T_C from the simple cubic (C) paraelectric to ferroelectric phases is composition dependent and changes almost linearly from ~400 K for pure $BaTiO_3$ (BT) to ~80 K for $x = 0.1$ (for lower x it becomes diffuse and disappears for the pure $SrTiO_3$ (ST), being only incipient ferroelectric and quantum paraelectric down to 0 K) [1–3]. The phase diagram of all three ferroelectric phases, well known from pure BT, is now rather well understood for the whole BST system both from thermodynamic [4] and microscopic theories [5, 6]. On decreasing temperature, BST becomes tetragonal (T), orthorhombic (O) and rhombohedral (R), the ferroelectric phases differing just by the direction of the spontaneous polarization P_s tending along the (100), (110) and (111) direction, respectively.

[4] Present address: Department of Physics, University of South Florida, Tampa, FL 33620, USA.
[5] Present address: Department of Physics of Science Faculty, IFIMUP, University of Porto, 4169-007 Porto, Portugal.

BST solid solution is nowadays very popular since it is the most promising system for microwave (MW) applications because of its high and well tunable dielectric permittivity with low dielectric losses [7]. For room temperature applications, the best systems correspond to the $x = 0.5$–0.6 compositions, where T_C is slightly below room temperature so that the material stays in the paraelectric C phase and has very high and strongly tunable permittivity combined with low dielectric losses, not deteriorated by ferroelectric domain-wall contributions [8]. Here we are going to discuss the dielectric and polar phonon behaviour only for the bulk BST samples (single crystals and dense ceramics). This should be a basis for better understanding the thin film behaviour, which is most important for applications, but is known to differ appreciably from bulk samples [7]. From this point of view, the dielectric properties of the C phase are the most interesting ones.

As early as 1970 the whole BST system was most thoroughly investigated in the MW range, both in the single-crystal as well as ceramic form (up to 72 GHz for some samples and in a broad 10–900 K temperature interval) by Bethe [9]. In the C phase, the measured temperature dependent MW losses in six BST single crystals of different compositions were compared with the anharmonic lattice dynamics theory for pure ST [10], yielding for the imaginary part $\varepsilon''(\omega, T)$ of the complex MW permittivity $\varepsilon(\omega, T) = \varepsilon' - i\varepsilon''$ a linear increase with frequency ω and a quadratic temperature T dependence in the C phase. A monotonic increase in losses was observed on increasing the Ba content x, in agreement with the intrinsic nature of the MW losses in these samples. The MW permittivity ε' in the C phase was frequency independent and equal to its low-frequency value obeying the Curie–Weiss law, in agreement with the assumed displacive nature of the ferroelectric transition in this system. In such systems a far infrared (IR) soft-phonon mode (SM) should be responsible for the total static temperature dependent permittivity values [11]. Even the expected bias electric field tunability of the MW permittivity was detected [9]. Close to T_C, however, some extra dielectric loss dispersion was observed in the GHz range for higher x (see figure 31 in [9]) and interpreted as a dipolar polarization contribution due to fluctuating polar regions, as later frequently observed close to various ferroelectric transitions [12, 13], in analogy to central mode (CM) phenomena in inelastic scattering experiments.

The ceramic system (seven different BST compositions were studied including pure BT and ST [9]) differed from that of single crystals only in additional GHz losses proportional to $1/\omega$, assigned to slightly more conductive grain boundaries (grain size $\sim$10 μm) and appreciable only for smaller x with smaller intrinsic losses. The bulk grain properties were assumed not to differ from single crystals. The latter assumption was recently thoroughly investigated and confirmed for pure ST ceramics with several grain sizes down to 80 nm [14, 15], even if the effective macroscopic dielectric response is substantially reduced with decreasing grain size due to low-permittivity grain-boundary dead-layer effects. The MW losses in BST crystals and ceramics were more recently analysed by Vendik *et al* [16].

Phonon properties on bulk BST were studied mainly by Raman scattering, both on single crystals [17] and ceramics [18–21]. Single-crystal Raman data and their comparison with those from BST thin films and BT/ST superlattices have been recently thoroughly reviewed by Tenne and Xi [22]. Concerning IR and THz spectroscopy, our data on ceramics for small $x \leqslant 0.2$ have already been published [23], as well as our preliminary data for the whole BST composition range ($x = 0.1, 0.2, 0.3, 0.4, 0.5, 0.6, 0.7, 0.8, 0.9$) [24]. Analogical data on pure ST and BT ceramics have been published, including their grain-size dependence [14, 15, 25].

In the C phase there are three IR-active F_{1u} transverse optical (TO) phonon modes (with increasing frequency TO1 (SM), TO2 and TO4), called Slater, Last and Axe modes, respectively, whose eigenvector consists of Ti versus O octahedra, Sr (Ba) versus TiO_6 octahedra and O_6-octahedron bending vibrations, respectively (the F_{2u} TO3 mode is silent) (see e.g. [26]). The main conclusion was that in the C phase—except for a temperature range close to T_C—the polar phonons (and electrons) contribute by the full value of the static permittivity so that no pronounced dielectric dispersion is expected in the MW and lower-frequency range. Therefore, the MW losses are low, as needed for MW applications. Close to T_C, however, an additional CM-like excitation is expected to contribute to relative permittivity (up to several thousands at T_C), peaked probably in the 10^2 GHz (1–10 cm^{-1}) range, whose parameters were not yet determined accurately. The presence of such a relaxation excitation (assigned to dipole polarization of polar nanoregions appearing close to T_C) was confirmed also from recent independent Fourier transform IR (FTIR), MW and radio-frequency (RF) experiments on BST-0.6 ceramics at room temperature [27] and very recently also in some temperature range around room temperature [28]. Its contribution to permittivity decreases in the C phase on heating, but remains appreciable up to $\sim$350 K. An analogical feature was recently observed even in the IR response of BT single crystals, where it was confirmed by molecular dynamics (MD) simulations with an effective Hamiltonian based on first-principles calculations [29].

In the ferroelectric phase, some additional MW and lower-frequency dispersion always appears in the permittivity [23, 24, 28], probably mainly due to the domain-wall dynamics. Still another source of MW and/or THz losses in the ferroelectric phase and also in the C phase under biasing electric field, so-called quasi-Debye losses, was suggested [30], based on the phonon transport theory [31], which, however, needs experimental verification. It is expected to produce an overdamped peak (relaxation) in the dielectric spectrum near the frequency of the SM damping. Since in BST the SM appears overdamped for higher x [24], the quasi-Debye response will be probably overlapped with the stronger SM response itself near T_C.

In this paper, we present and discuss our new THz transmission and IR reflectivity data on a coarse-grain BST-0.6 ceramic, complemented by MW and lower-frequency dielectric measurements, in a broad temperature range in paraelectric as well as all the three ferroelectric phases. The anomalous SM response is also calculated from first-principles effective Hamiltonian molecular dynamics (MD) simulations [24, 29]. Comparison of the obtained results

offers a consistent interpretation of the dielectric spectra in this important MW material.

2. Experimental details

BST-0.6 ceramic samples were prepared by the conventional mixed-oxide route. Reagent grade $SrCO_3$, TiO_2 and $BaCO_3$ were weighed according to the $Sr_{1-x}Ba_xTiO_3$ compositions with $x = 0.6$. After ball milling in alcohol for 5 h, using Teflon pots and zirconia balls in a planetary mill, the powders were dried, and then calcined at 1100 °C for 5 h. The calcined powders were milled again for 5 h, to obtain powders with particle size lower than 5 μm. Pellets of 10 mm in diameter were uniaxially pressed at 100 MPa and then isostatically pressed at 200 MPa. Sintering was performed in air at 1500 °C for 5 h, yielding a density of the ceramic samples of ∼97% of the theoretical density.

Room temperature XRD analysis (Rigaku D/Max-B, Cu Kα), conducted on the ground sintered samples, indicated single-phase perovskite structure. The microstructure and chemical analysis of ceramics were performed on polished and thermally etched sections using SEM/EDS (Hitachi S-4100), revealing an average grain size of about 40 μm.

The dielectric measurements at 10 kHz were performed on polished 1.5 mm thick pellets 8 mm in diameter in a He closed-cycle cryogenic system Displex ADP-Cryostat HC-2, using the HP 4284A precision LCR meter. Dielectric measurements in the 1 MHz–1.8 GHz range were performed using a computer-controlled dielectric spectrometer equipped with an Agilent 4291B impedance analyser, Novocontrol BDS 2100 coaxial sample cell and Sigma System M18 temperature chamber (operating range 100–500 K). Special cylindrical samples (8 mm long and 1 mm in diameter) with Au electrodes sputtered on their bottom and top surfaces were prepared from the pellets to match the impedance range of the analyser. Such geometry enabled us to perform measurements on our high-permittivity material up to 1.8 GHz (accuracy ∼5%). The dielectric parameters were calculated taking into account the electromagnetic field distribution in the sample. MW dielectric properties were measured at 8.8 GHz on the same sample, inserted in the TE_{0n1} composite dielectric resonator [32], using an Agilent E8364B vector network analyser and Sigma System M18 temperature chamber (100–380 K). The estimated accuracy of our MW measurements is ∼10%.

IR spectra were obtained using an FTIR spectrometer Bruker IFS 113v in the frequency range of 20–3300 cm^{-1} (0.6–100 THz). Terahertz (THz) spectra were obtained by means of time-domain THz transmission spectroscopy on plane-parallel plates of 8 mm diameter thinned to 35 μm. For these experiments we used a Ti:sapphire femtosecond laser oscillator. Linearly polarized THz probing pulses were generated by an interdigitated photoconducting switch [33] and detected using the usual electro-optic sampling scheme with a 1 mm thick [110] ZnTe crystal plate [34]. Both the transmitted field amplitude and phase shift were simultaneously measured, allowing us to determine directly the complex dielectric response $\varepsilon^*(\omega)$ in the range from 5 to 30–70 cm^{-1} (depending on temperature). The measurements were performed in the 5–800 K temperature range. An Optistat (Oxford Instruments) continuous-flow cryostat with polyethylene (FTIR) or Mylar (THz) windows was used for cooling and a high-temperature cell Specac P/N 5850 for heating.

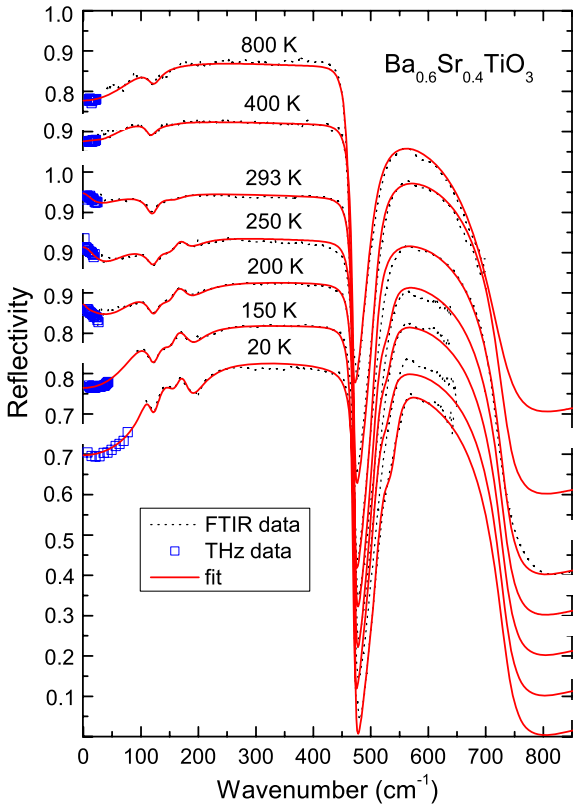

Figure 1. Normal reflectivity spectra at several selected temperatures. Comparison of experimental data (empty squares evaluated from THz spectra, dotted lines FTIR reflectivity) with fitting curves (solid lines).

All the spectra were measured on cooling. At low, high and MW frequencies the data were detected during slow cooling with a temperature rate 0.5–1 K min^{-1}, while the THz and IR spectra were taken at fixed stabilized temperatures with an interval of 10–100 K.

3. Results, evaluations and calculations

The low-frequency dielectric measurements have shown typical permittivity values and anomalies corresponding to the C–T transition at $T_C = 273$ K and also revealed the T–O transition near 210 K and also O–R transition near 160 K.

IR reflectivity spectra for selected temperatures are plotted in figure 1 together with their fitting curves. The experimental $R(\omega)$ data below ∼50 cm^{-1} are calculated from the complex THz permittivity spectra $\varepsilon^*(\omega)$ using the relation

$$R(\omega) = \left| \frac{\sqrt{\varepsilon^*(\omega)} - 1}{\sqrt{\varepsilon^*(\omega)} + 1} \right|^2. \quad (1)$$

IR reflectivity and THz dielectric spectra were fitted simultaneously using the generalized oscillator model with the

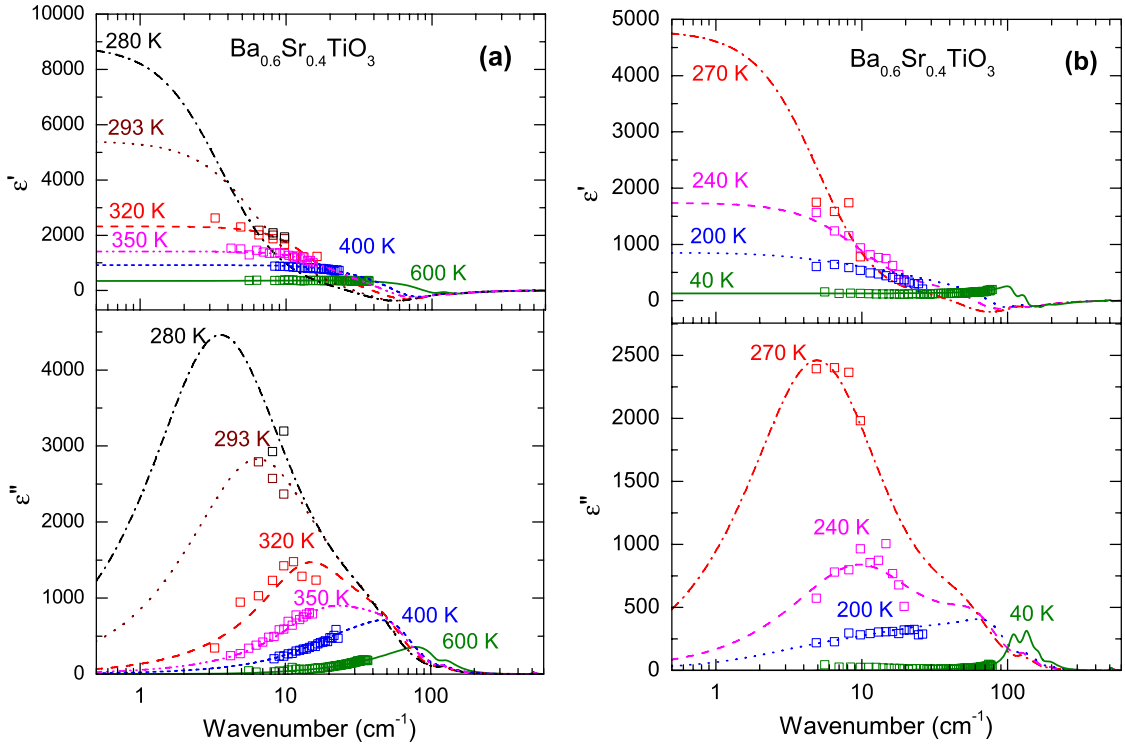

Figure 2. Complex permittivity from the IR reflectivity fits together with the THz data in the paraelectric (a) and ferroelectric (b) phase.

factorized form of the complex permittivity

$$\varepsilon^*(\omega) = \varepsilon_\infty \prod_{j=1}^{n} \frac{\omega_{\mathrm{LO}j}^2 - \omega^2 + \mathrm{i}\omega\gamma_{\mathrm{LO}j}}{\omega_{\mathrm{TO}j}^2 - \omega^2 + \mathrm{i}\omega\gamma_{\mathrm{TO}j}}. \qquad (2)$$

Here $\omega_{\mathrm{TO}j}$ and $\omega_{\mathrm{LO}j}$ mark the transverse and longitudinal frequencies of the jth mode, respectively, and $\gamma_{\mathrm{TO}j}$ and $\gamma_{\mathrm{LO}j}$ denote their corresponding damping constants. We estimated the high-frequency permittivity, originated from electronic absorption processes at much higher frequencies than phonon frequencies (typically in the UV–vis range), as $\varepsilon_\infty = 5.4$, and neglected its very small temperature dependence in our fits.

Figure 1 demonstrates that the spectra above 300 cm^{-1} do not change appreciably with temperature. The highest phonon band at 480–750 cm^{-1} (Axe mode), shows some splitting below T_C, but its frequency remains practically temperature independent in the whole temperature range. The lowest very broad restrahl band (∼30–470 cm^{-1}), corresponding to the Slater mode, exhibits maximal values (above 90% of reflectivity) close to T_C and continuously reduces its low-frequency wing on cooling and on heating. The Last-type TO2 vibration manifests itself by a very weak broad minimum inside the Slater band at about 165 cm^{-1}. It is slightly lower than its position in the pure ST and BT and, unlike in these compounds, it is hardly distinguishable in the reflectivity spectra and practically unresolved in the dielectric response. In previous studies [2, 17, 24, 25] the presence of an extra mode at 120–130 cm^{-1} specific for the BST-solution has been already reported. Its presence was assigned to a disorder activated (DA) acoustic phonon from the Brillouin-zone boundary. We also see this mode in the whole temperature range as a clear minimum inside the Slater restrahl band.

In the wide temperature interval around T_C (180–500 K) we observe an additional low-frequency band in $R(\omega)$ close below the polar phonon dispersion and assign it to a CM-type excitation. In the complex dielectric function spectra, shown together with the THz data in figure 2, this CM strongly overlaps with the TO1 SM so that the corresponding peak in the loss function $\varepsilon''(\omega)$ looks like one asymmetric band. Just above T_C the CM band dominates in the dielectric response (figure 2(a)). The position of the peak is strongly temperature dependent and hardens on heating from ∼3.5 cm^{-1} (0.1 THz) at 280 K up to ∼24 cm^{-1} at 350 K. It gradually weakens on heating and merges with the SM frequency at higher temperatures. Above 500 K, the CM response completely disappears from our fit and a single-oscillator fit describes well the SM response.

Below T_C (figure 2(b)), due to the expected strong lattice anisotropy, the mode degeneracy is lifted either completely (in the O phase) or partially (in the T and R phases). Splitting of the polar F_{1u} phonons is, however, negligible in the case of the Last mode, and we do not consider it either for the Axe mode. So, further we shall discuss only splitting of the Slater F_{1u}(TO1) mode into E and A_1 components in the T and R phase, and into B_2, B_1 and A_1 components in the O phase. To estimate it more quantitatively, in ceramics and multi-domain samples we are able to measure only the so-called effective response, averaged over small single crystalline regions with all possible orientations. Even if we expect to see in our effective spectra all the polar modes, their mode strengths as well as frequencies are affected by the averaging. Still, in agreement with Raman data [17, 22], the appearance of the A_1 Slater mode component at about 200 cm^{-1} below

T_C and its strengthening on cooling is quite well observable in our reflectivity spectra (figure 1). The redistribution of the CM strength between the E and A_1 spectra remains, however, unclear, even if the CM contribution (0.1–30 cm^{-1}) prevails in the dielectric spectra down to the O phase. In the O phase, the SM degeneracy is fully lifted and three A_1, B_1 and B_2 components are seen. The lowest B_2 phonon, lying below ~40 cm^{-1}, is probably overlapping with the CM and the two contributions cannot be unambiguously separated. In the R phase below 160 K, the CM-type dispersion vanishes. This is due to the fact that all SM components become rather hard, in analogy with BT, which is known to have fully ordered Ti ions in this phase [35].

To shed more light on the origin of this complicated response of various soft-mode components, we also performed MD simulations of BST-0.6 using the effective Hamiltonian model of [6]. While the parameters of this atomistic model were derived from first-principles calculations based on local density functional theory, the only dynamic degrees of freedom of this model were inhomogeneous and homogeneous strain variables and 'local soft modes' associated with the lowest optical phonon branch. Simulations of disordered BST with a prescribed concentration were carried out by placing randomly the Ba and Sr atoms inside a supercell (typically 16 × 16 × 16 perovskite unit cells). Thus, the model assumed only a single dynamical polar degree of freedom per unit cell (local Slater-type mode coordinate). In spite of these simplifications, the model reproduced fairly well the composition–temperature phase diagram of BST disordered solid solutions [6] in a wide composition range and it was also successfully used to mimic the complex dielectric response of the soft mode in crystals of pure BT [29, 36].

The complex dielectric response of BST-0.6 was calculated exploiting direct MD simulations with this model using the scheme of [24, 29]. The initial state was typically prepared using equilibration cycle with 40 000 MD steps at constant number of particles, pressure and temperature (*NPT* ensemble) and 5000 MD steps at fixed number of particles, volume and energy (*NVE* ensemble). About 2.4×10^8 individual MD steps with 1 fs duration were then used to calculate the total dipole moment of the supercell as a function of time. The complex dielectric response was calculated from the Fourier transform of the total dipole moment autocorrelation function. To smooth out the calculation noise, resulting spectra of complex permittivity were fitted to the sum of damped harmonic oscillators.

Taking into account the simplicity of the model, we could not expect a perfect reproduction of the experimental spectra by MD simulations. For us, predicting a temperature behaviour of the CM–SM response qualitatively similar to the observed one could already be considered as a success of our theoretical approach. Indeed, our simulated complex dielectric function showed strong SM softening close to T_C and splitting into two components. In figure 3, we compare the complex dielectric function fitted to experimental data and obtained from MD simulation at two selected temperatures above T_C (320 and 600 K). Splitting of the low-frequency band into CM and SM at 320 K is clearly seen in both the theory and

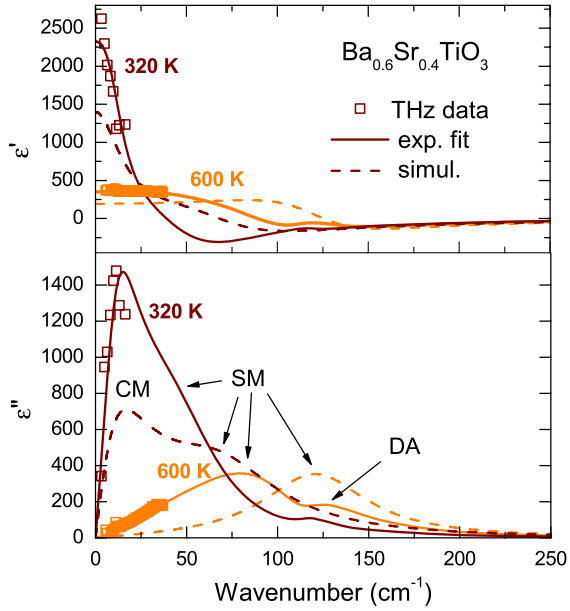

Figure 3. Real and imaginary part of the complex dielectric function: comparison of the fitting spectra (solid lines) and MD simulations (dashed lines) for two selected temperatures (320 and 600 K).

experiment, while at 600 K the splitting disappears and the loss maximum shifts to higher frequencies in both cases. This semi-quantitative agreement strongly supports the intrinsic nature of the dielectric dispersion for frequencies at least down to about 200 GHz.

In the ferroelectric phases, the simulated dielectric response is anisotropic and dielectric tensor components along the high symmetry directions show very distinct spectra. In order to mimic the effective response of the corresponding ceramic material, we have combined the spectra corresponding to the principal dielectric axes into a single spectrum using a simple effective medium mixing formula (geometric mean model [37]), first proposed by Lichtenecker [38]:

$$K = \prod_{l=1}^{s} K_l^{\Theta_l}, \tag{3}$$

where K_l is the lth component of a response function (here complex permittivity) and θ_l is the corresponding volume fraction. We took $\theta = 0.33$ for A_1, B_1 and B_2 responses and $\theta = 0.66$ for the E response, with $s = 2$ in T and R phases and $s = 3$ in the O phase.

For comparison of the lattice contributions in a broad temperature range we used for convenience the real part of the optical conductivity (see figure 4), proportional to $\omega\varepsilon''(\omega)$ [26]. The contribution of a mode described as an independent damped harmonic oscillator appears here as a deformed Lorentzian with its maximum positioned precisely at the TO frequency (even for overdamped oscillators) and the peak area of each oscillator contribution is proportional to its oscillator strength. Calculated effective conductivity spectra showed similar temperature evolution to those obtained from experiment: softening of the SM on both sides of T_C and its splitting into two components in the vicinity of T_C. The main

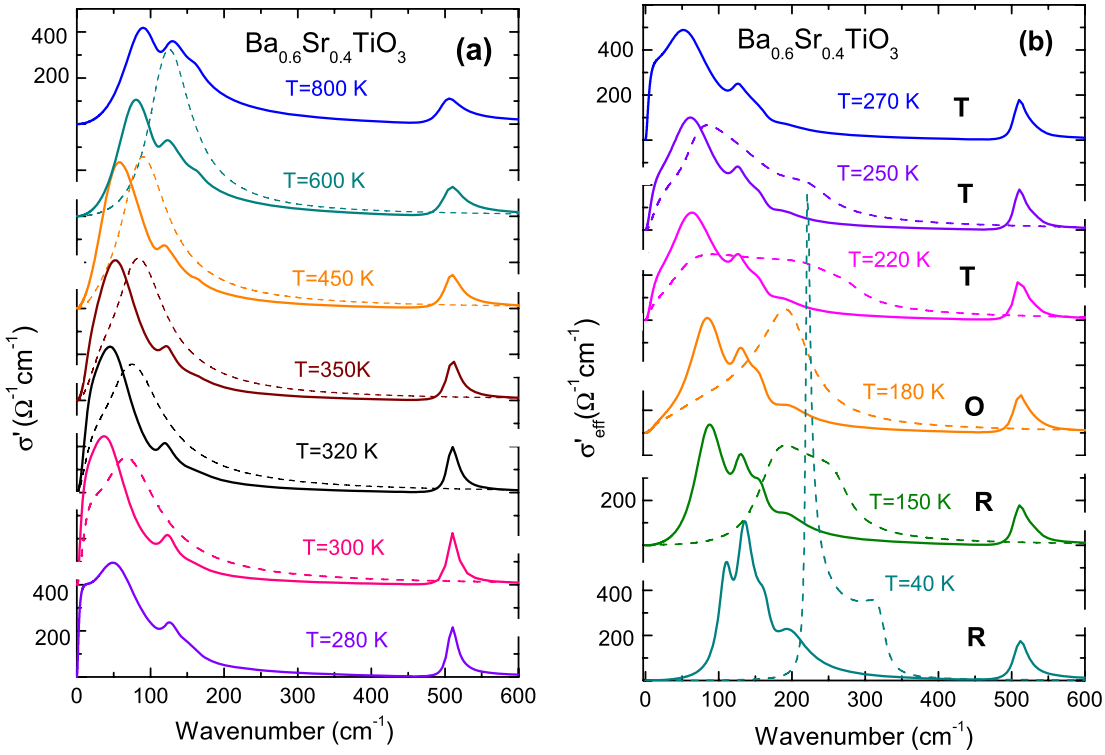

Figure 4. Real part of the optical conductivity at selected temperatures above (a) and below (b) T_C. Solid lines, fit to experiment; dashed lines, MD simulated spectra.

quantitative difference consists in a harder SM response and its stronger hardening below T_C in the theory. We think that this effect can be at least partially explained by the coupling of the Slater mode with the other modes, which is not considered by the simulation.

Our dielectric measurements down to 1 MHz did not show any appreciable dispersion below the phonon frequencies in the paraelectric phase (figure 5(a)). Just very close to T_C a significant broad relaxation started to appear in the GHz range. We also indicated some increase of $\varepsilon''(\omega)$ in the MHz range but this low-frequency dispersion practically did not influence the values of $\varepsilon'(\omega)$. Below T_C (figure 5(b)), the GHz dispersion became dominating in the dielectric spectra. In the fit of our data, which is shown in figure 5, we included two oscillator terms, representing soft optic phonons, and two Cole–Cole relaxations [39] for describing the GHz and MHz dispersion, which are too broad to be described by the Debye relaxation terms. Due to the lack of data in the 10–100 GHz range and below 1 MHz, this fit cannot be considered as unambiguous. Nonetheless, below T_C it clearly indicates the presence of a strong and broad relaxation in the GHz range, which narrows on cooling, approaching the simple Debye relaxation, and a weaker and more smeared relaxation with the loss maximum at about or below 1 MHz. Within the accuracy of our fit we did not observe any significant temperature dependence of the relaxation frequencies and consider both relaxations as extrinsic loss mechanisms. Without any deeper study, we could assign the stronger GHz dispersion to the domain-wall contribution pinned by the grain boundaries and/or to the smeared piezoelectric resonances on the grain boundaries.

4. Discussion

In figure 6, we plotted the temperature dependence of the TO frequencies (a), dampings (b) and oscillator strengths (squares of their plasma frequencies $\Omega_i = \sqrt{\Delta\varepsilon_i\omega_i^2}$ [26]) (c) obtained from the fit of our experimental spectra with the factorized dielectric function (equation (1)). The mode at about 165 cm^{-1}, which we assign to the Last-type F_{1u} phonon, and the DA mode at about 125 cm^{-1} (acoustic mode from the Brillouin-zone boundary), do not show any substantial temperature dependences of their frequencies, neither splitting below T_C. The activation of the DA mode most probably originates from the local tilting of oxygen octahedra, caused by the alternating compressing and expanding of the Ba- and Sr-filled unit cells. The Slater F_{1u} mode softens on approaching T_C and splits into the A_1 and E components below T_C, but its softening is rather weak due to the appearance of the CM-band below it. Due to the ambiguity of the TO frequency caused by the strong SM and CM dampings, we also plot their dampings in figure 6(b). Strong increase of the SM frequency and reduction of its damping proves the complete Ti ion ordering in the R phase, known for the pure BT [35].

Figure 6(c) indicates that far from T_C, where the SM band approaches the DA peak, the latter significantly takes over its oscillator strength. In the vicinity of T_C, the main strength interchange takes place between SM and CM: it is quite clear that the CM peak appears and strengthens at the expense of the SM. Such behaviour is a classical example of an SM–CM coupling in the vicinity of a displacive phase transition with order–disorder crossover [12]. The fact that the total

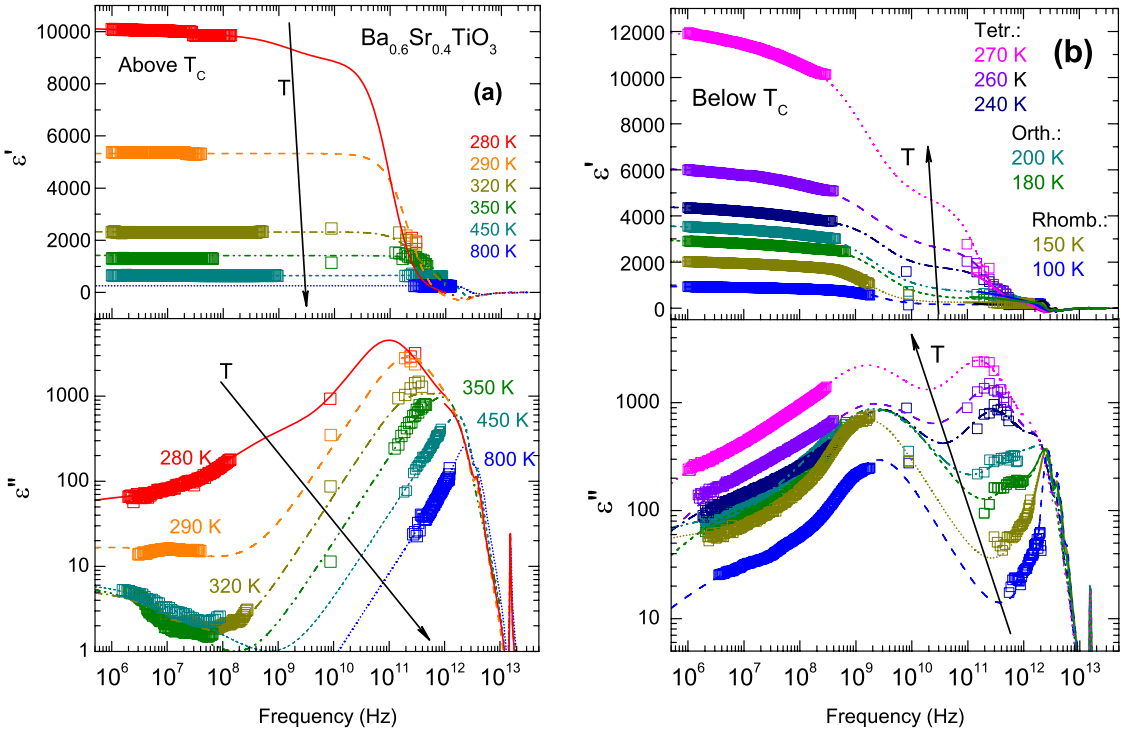

Figure 5. Broad-band spectra of BST-0.6 at selected temperatures above (a) and below (b) T_C.

oscillator strength of all the polar phonon modes, calculated as $\Omega^2_{\text{total}} = \sum_i \Omega_i^2$, remains temperature independent brings evidence that the sum rule for the polar modes is valid and coupling to other excitations can be neglected. Moreover, it proves the good accuracy of our experiment and consistency of its fitting.

In order to describe the coupling of the SM and CM modes more quantitatively, we modelled our experimental complex dielectric response spectra in the 1–200 cm^{-1} range from T_C up to 450 K by a coupled Debye relaxation (representing the CM) and Lorentzian oscillator (SM) neglecting the sharper DA mode contribution. We used the simplest coupled-mode expression [40, 41]:

$$\varepsilon(\omega) = S_i S_j G_{ij}(\omega) + \varepsilon_\infty, \tag{4}$$

where $\boldsymbol{G}(\omega)$ is a Green function matrix of the coupled modes with a real bilinear coupling constant δ, vector $\boldsymbol{S}$ describes the dielectric strength of the two modes and ε_∞ now reflects the high-frequency permittivity, including the contribution of higher-frequency polar modes.

$$G^{-1}(\omega) = \begin{pmatrix} 1 - \mathrm{i}\omega/\gamma & \delta \\ \delta & \omega_0^2 - \omega^2 - \mathrm{i}\omega\Gamma \end{pmatrix}, \tag{5}$$

where ω_0 and Γ are the bare SM eigenfrequency and damping, respectively, and γ is the CM relaxation frequency. In our approach, we assumed a zero bare strength of the Debye relaxation with temperature independent bare frequency (33 cm^{-1}) so that the CM activates in the THz spectra only owing to its coupling to the SM. In figure 7, we show the temperature dependence of the parameters of the bare SM and δ. As expected, SM only partially softens and its coupling with CM slightly increases on approaching T_C. This fit shows that the polar phonon dynamics of BST-0.6 is close to the crossover between displacive and order–disorder dynamics known from several ferroelectrics [12], including also the recently revealed CM-type dynamics in pure BT crystals [29, 36]. As in BT, the specific feature here is the very high frequency of the CM response, which lies in the THz range and strongly overlaps with the SM response.

In figure 8, we compare the dielectric contributions from polar phonons including CM with that of relaxation contributions in the whole studied temperature range. It shows almost pure lattice dispersion in the C phase and appearance of significant relaxation dispersion only very close to T_C. In the ferroelectric phase, however, the relaxation contributions are prevailing in spite of its weakening on cooling. Note the perfect agreement between the contribution to permittivity from our fit of the high-frequency data and the directly measured low-frequency permittivity. This strongly supports the reasonability of our fit.

The ultra-broad dielectric response of BST-0.6 ceramics around T_C has been investigated by similar experimental methods (except for the THz transmission spectroscopy) in a very recent independent work of Teranishi *et al* [28]. They also observed a contribution analogical to our CM already in the C phase. Teranishi *et al* assigned it to a dipolar polarization of dynamic polar clusters. This agrees with our understanding of the origin of the CM; see the corresponding discussion for BT in [36]. However, unlike our CM contribution (see figure 8), the dipolar contribution to permittivity evaluated in [28] shows no maximum at T_C and continues to increase in the ferroelectric phase (see figure 3 there). We believe that this is caused by much lower accuracy of the FTIR

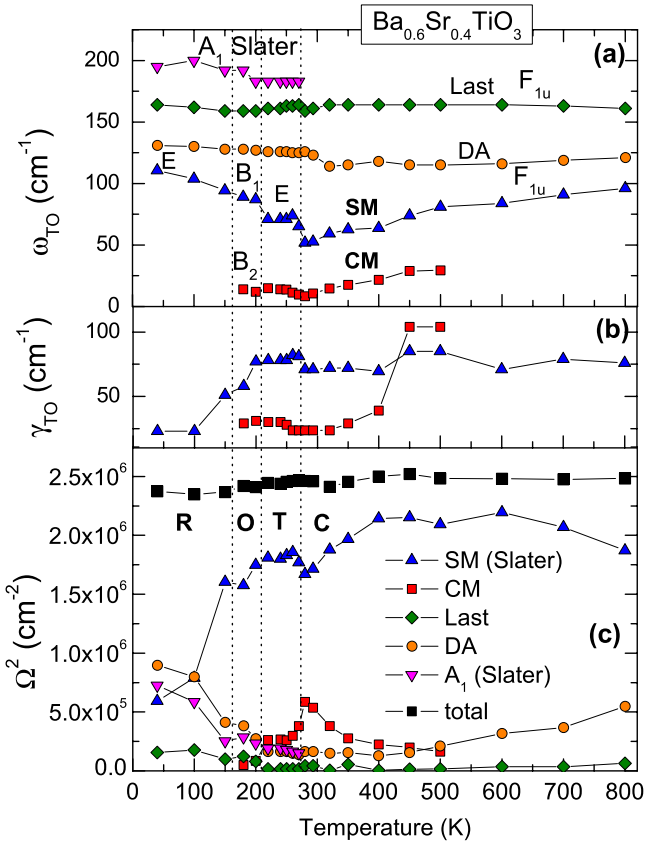

Figure 6. Temperature evolution of the parameters (ω_{TO} (a), γ_{TO} (b), and oscillator strength (c)) used for the fit of experimental spectra by the factorized four-parameter damped harmonic oscillator model.

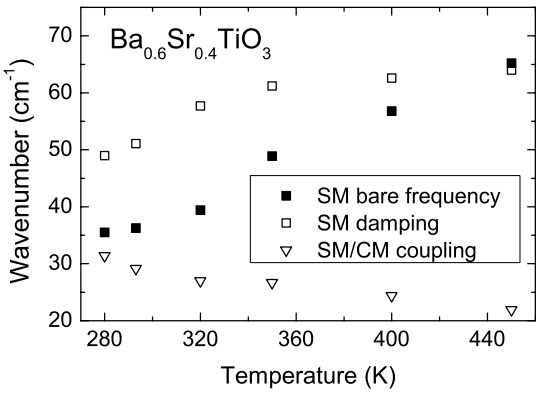

Figure 7. Bare SM parameters, evaluated from the fit of the dielectric spectra by the model of coupled SM and CM.

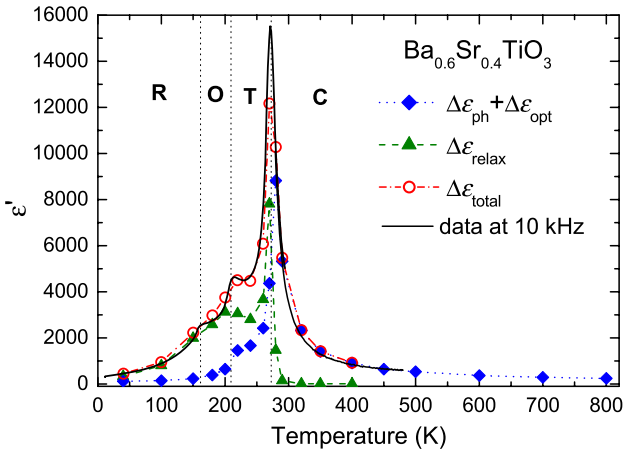

Figure 8. Comparison of phonon and relaxation contributions to the static dielectric permittivity.

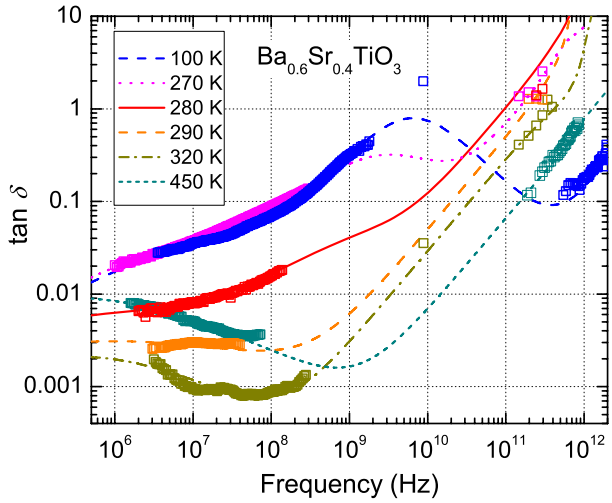

Figure 9. Frequency dependence of the loss tangent at selected temperatures. Symbols (empty squares) indicate experimental data; lines show our fit to experiment.

reflectivity measurements at their low-frequency end compared to our THz transmission measurements and the way in which their data were modelled in the frequency region where they had no reliable data. Indeed, the authors of [28] assumed a single overdamped damped harmonic oscillator contribution where we have placed two contributions—CM and SM. The peak frequency in the $\varepsilon''(\omega)$ spectra in figure 2 of [28] is appreciably lower than in our spectra (see figure 5). In particular, due to our better sensitivity of THz transmission measurements, we could measure the permittivity up to about 3000 with a comparably high imaginary part, whereas the fitted permittivity data of [28] yield only several hundred in the same frequency range. Otherwise, both sets of data are in fairly good agreement.

Finally, in figure 9 we plot the frequency dependence of the loss tangent from our fits for several selected temperatures. The linear increase at high frequencies in the C phase corresponds to intrinsic losses due to the low-frequency tails of SM and CM, as expected theoretically [7]. The levelling off or even a loss increase at low frequencies is obviously due to extrinsic losses, probably caused by grain boundaries, as analysed already by Bethe [9]. But the intrinsic values at 10 GHz are of the same order of magnitude as those for the BST-0.65 single crystals [8, 9]. They show that in a quite broad 1–100 GHz range the minimum loss tangent in BST ceramics should be expected to be about 100–150 K above T_C. Since the tunability of permittivity reaches its maximum close to T_C, the temperature of the optimal regime for applications needs some compromise. The tunability and intrinsic losses were analysed

in detail for ST and BST-0.6 by Astafiev *et al* [30], where it was shown that, unlike in ST, in the case of BST the quasi-Debye losses induced in the paraelectric phase by the electric field are negligible and therefore the BST material is more suitable for room temperature applications than the pure ST even at low temperatures.

5. Conclusions

In the present work we have carried out a detailed study of the dispersion mechanisms in BST-0.6 in a broad frequency and temperature range in all the known phases. We demonstrated that above T_C the dielectric function is of an almost pure phonon character with the dominating SM–CM dispersion in the THz frequency range. This type of dispersion can be described by a simple model of a bilinearly coupled SM oscillator with a temperature independent silent Debye relaxation representing the CM. Its existence was also confirmed by MD simulations based on the first-principles effective Hamiltonian. Below T_C, additional important dispersion, assigned to domain-wall dynamics, appears in the GHz range. It is demonstrated that in the paraelectric phase the BST-0.6 ceramic is suitable for MW application in a broad frequency range.

Acknowledgments

The authors acknowledge the support from MSMT project ME08109, ASCR AVOZ10100520 and A100100907; NSF grants DMR-0701558, DMR-0404335 and DMR-0080054 (C-SPIN) and ONR grants N00014-04-1-0413 and N00014-08-1-0915. We also acknowledge the computational support provided by NSF MRI grant 072265, and by the HPCMO of the US DoD.

References

[1] Jona F and Shirane G 1962 *Ferroelectric Crystals* (Oxford: Pergamon)
[2] Lemanov V V, Smirnova E P, Syrnikov P P and Tarakanov E A 1996 *Phys. Rev.* B **54** 3151
[3] Menoret C, Kiat J M, Dkhil B, Dunlop M, Dammak H and Hernandez O 2002 *Phys. Rev.* B **65** 224104
[4] Shirokov V B, Torgashev V I, Bakirov A A and Lemanov V V 2006 *Phys. Rev.* B **73** 104116
[5] Tinte S, Stachiotti M G, Phillpot S R, Sepliarsky M, Wolf D and Migoni R L 2004 *J. Phys.: Condens. Matter* **16** 3495
[6] Walizer L, Lisenkov S and Bellaiche L 2006 *Phys. Rev.* B **73** 144105
[7] Tagantsev A K, Sherman V O, Astafiev K F, Venkatesh J and Setter N 2003 *J. Electroceram.* **11** 5
[8] Vendik O G, Hollmann E K, Kozyrev A B and Prudan A M 1999 *J. Supercond.* **12** 325
[9] Bethe K 1970 *Philips Res. Rep.* (Suppl. no. 2) 1 (in German)
[10] Silverman B D 1962 *Phys. Rev.* **125** 1921
[11] Cochran W 1959 *Phys. Rev. Lett.* **3** 412
[12] Petzelt J, Kozlov G V and Volkov A A 1987 *Ferroelectrics* **73** 101
[13] Buixaderas E, Kamba S and Petzelt J 2004 *Ferroelectrics* **308** 131
[14] Petzelt J, Ostapchuk T, Gregora I, Nuzhnyy D, Rychetsky I, Maca K and Shen Z 2008 *Ferroelectrics* **363** 227
[15] Petzelt J, Ostapchuk T, Gregora I, Kuzel P, Liu J and Shen Z 2007 *J. Phys.: Condens. Matter* **19** 196222
[16] Vendik O G, Zubko S P and Nikolski M A 2002 *J. Appl. Phys.* **92** 7448
[17] Tenne D A, Soukiassian A, Xi X X, Choosuwan H, Guo R and Bhalla A S 2004 *Phys. Rev.* B **70** 174302
[18] Lemanov V V 1997 *Phys. Solid State* **39** 318
[19] Naik R, Nazarko J J, Flattery C S, Venkateswaran U D, Naik V M, Mohammed M S, Auner G W, Mantese J V, Schubring N W, Micheli A L and Catalan A B 2000 *Phys. Rev.* B **61** 11367
[20] Kuo S-Y, Liao W-Y and Hsieh W-F 2001 *Phys. Rev.* B **64** 224103
[21] Katiar R S, Jain M and Yuzyuk Yu I 2004 *Ferroelectrics* **303** 101
[22] Tenne D A and Xi X X 2008 *J. Am. Ceram. Soc.* **91** 1820
[23] Ostapchuk T, Savinov M, Petzelt J, Pashkin A, Dressel M, Smirnova E, Lemanov V, Sotnikov A and Weihnacht M 2007 *Ferroelectrics* **353** 504
[24] Ostapchuk T, Petzelt J, Kuzel P, Veljko S, Tkach A, Vilarinho P, Ponomareva I, Bellaiche L, Smirnova E, Lemanov V, Sotnikov A and Weihnacht M 2008 *Ferroelectrics* **367** 139
[25] Ostapchuk T, Petzelt J, Savinov M, Buscaglia V and Mitoseriu L 2006 *Phase Transit.* **79** 361
[26] Hlinka J, Petzelt J, Kamba S, Noujni D and Ostapchuk T 2006 *Phase Transit.* **79** 41
[27] Tsurumi T, Li J, Hoshina T, Kakemoto H, Nakada M and Akedo J 2007 *Appl. Phys. Lett.* **91** 182905
[28] Teranishi T, Hoshina T, Takeda H and Tsurumi T 2009 *J. Appl. Phys.* **105** 054111
[29] Ponomareva I, Bellaiche L, Ostapchuk T, Hlinka J and Petzelt J 2008 *Phys. Rev.* B **77** 012102
[30] Astafiev K F, Tagantsev A K and Setter N 2005 *J. Appl. Phys.* **97** 014106
[31] Gurevich V L and Tagantsev A K 1991 *Adv. Phys.* **40** 719
[32] Krupka J, Zychovicz T, Bovtun V and Veljko S 2006 *IEEE Trans. Ultrason. Ferroelectr. Freq. Control* **53** 1883
[33] Dreyhaupt A, Winnerl S, Dekorsy T and Help M 1996 *Appl. Phys. Lett.* **69** 2321
[34] Nahata A, Weling A S and Heinz T F 1996 *Appl. Phys. Lett.* **69** 2321
[35] Luspin Y, Servoin J L and Gervais F 1980 *J. Phys. C: Solid State Phys.* **13** 3761
[36] Hlinka J, Ostapchuk T, Nuzhnyy D, Petzelt J, Kuzel P, Kadlec C, Vanek P, Ponomareva I and Bellaiche L 2008 *Phys. Rev. Lett.* **101** 167402
[37] Zakri T, Laurent J-P and Vauclin M 1998 *J. Phys. D: Appl. Phys.* **31** 1589
[38] Lichtenecker K 1926 *Z. Phys.* **27** 115
[39] Jonscher A K 1983 *Dielectric Relaxation in Solids* (London: Chelsea Dielectric Press)
[40] Reese R L, Fritz I J and Cummins H Z 1973 *Phys. Rev.* B **7** 4165
[41] Kadlec C, Kadlec F, Nemec H, Kuzel P, Schubert J and Panaitov G 2009 *J. Phys.: Condens. Matter* **21** 115902